https://doi.org/10.5194/amt-2020-43
Preprint. Discussion started: 27 February 2020

Atmospheric Measurement Techniques Discussions

Commercial Microwave Links as a tool for operational rainfall monitoring in Northern Italy

Giacomo Roversi[1], Pier Paolo Alberoni[2], Anna Fornasiero[2], and Federico Porcù[1]

[1]Department of Physics and Astronomy, University of Bologna, Bologna, 40100, Italy
[2]Arpae-SIMC, Bologna, 40100, Italy

Correspondence: Federico Porcù (federico.porcu@unibo.it)

Abstract. There is a growing interest in emerging opportunistic sensors for precipitation, motivated by the need to improve its quantitative estimates at the ground. In this work a preliminary assessment of the accuracy of Commercial Microwave Links (CMLs) retrieved rainfall rates in northern Italy is presented. The CML product, obtained by the publicly available RAINLINK package, is evaluated at different scales (single link, $5\mathrm{km}\times5\mathrm{km}$ grid, river basin) against the precipitation products operationally used at Arpae-SIMC, the Regional Weather Service of Emilia-Romagna, in northern Italy. The results of the 15 min single-link validation with close-by raingauges show high variability, with influence of the area physiography and precipitation patterns and the impact of some known issues (e.g. melting layer). However, hourly cumulated spatially interpolated CML rainfall maps, validated with respect to the established regional gauge-based reference, show performances (R^2 of 0.47 and CV of 0.77) which are very similar, when not even better, to satellite- and adjusted radar-based precipitation gridded products. This is especially true when basin-scale total precipitation amounts are considered (R^2 of 0.85 and CV of 0.63). A diffuse underestimation is evident at both grid box (Mean Error of -0.26) and basin scale (Multiplicative Bias of 0.7), while the number of false alarms is generally low and gets even lower as coverage increases. Taking into account also delays in the availability of the data (latency of 0.33 hours for CML against 1 hour for the adjusted radar and 24h for the quality controlled raingauges), CMLs appear as a valuable data source in particular from a local operational framework perspective. Finally, results show complementary strengths for CMLs and radars, encouraging a joint exploitation.

1 Introduction

Precipitation is one of the most difficult geophysical observables to measure and monitor, given its very high temporal and spatial variability. Its accurate measurement would benefit a wide range of applications in meteorology, hydrology, climatology, agriculture, just to mention the most direct fields where precipitation plays a key role. The precipitation rate can be measured or estimated directly at the ground or by means of different remote sensing approaches. Rain gauge networks provide point-like measurements of the amount of rain fallen within the instrument's sampling area, cumulated over time intervals which usually

https://doi.org/10.5194/amt-2020-43
Preprint. Discussion started: 27 February 2020

Atmospheric Measurement Techniques Discussions

range from one minute to one day, with well known instrumental constraints (Lanza and Stagi, 2012) and representativeness limitations (Porcù et al., 2014). Ground based weather radars, often deployed in large scale networks (Serafin and Wilson, 2000; Huuskonen et al., 2014; Saltikoff et al., 2019), are widely used by hydro-meteorological services to quantitatively monitor precipitation fields, being an effective trade off between spatial-temporal coverage and accuracy in the measurements. However, radar estimates are affected by a number of errors, which the last generation polarimetric systems have only partially mitigated (Ryzhkov and Zrnic, 2019). Satellite estimates received a renewed boost in the last decade from the full exploitation of the Global Precipitation Measurement mission (GPM, Skofronick-Jackson et al. (2017)) that operationally releases a new suite of precipitation products with high temporal and spatial resolution (Mugnai et al., 2013; Grecu et al., 2016). Despite the undoubted potentials of satellite products to provide estimates over open oceans and regions not equipped with ground instruments, their accuracy is still under evaluation (Tan et al., 2018) and their latency hinders the use in real time monitoring of rain patterns.

A relatively new and independent approach to the estimates of precipitation at the ground became available in the last decades with the broad diffusion of microwave links for cellular communication (or Commercial Microwave Links, CMLs): integral precipitation content along a straight path between two antennas can be estimated by measuring the attenuation of the microwave signal travelling down the same path (Turner and Turner, 1970; Harden et al., 1978). Accurate algorithms were introduced to measure average rainfall rates (Rahimi et al., 2003), drop size distribution (Rincon and Lang, 2002; van Leth et al., 2019) and water content (Jameson, 1993) along the link. The possibility to have a spatially continuous rainfall path depends on the density and distribution of the links, making this approach of particular interest for urban areas (Upton et al., 2005; Overeem et al., 2011; Fenicia et al., 2012; Fencl et al., 2013; Rios Gaona et al., 2017; de Vos et al., 2018) with also direct hydrological use in combination with conventional instruments (Grum et al., 2005; Fencl et al., 2013). A further application of CML approach could be in regions where other instruments are lacking or absent at all (Mulangu and Afullo, 2009; Abdulrahman et al., 2011; Doumounia et al., 2014). However, as it happens for conventional precipitation instruments, the quality of the retrieval is sensitive to a number of factors often difficult to control (Leijnse et al., 2008) and to the precipitation micro-physical structure (Berne and Uijlenhoet, 2007; Leijnse et al., 2010). Given these limitations intrinsic to the measurement geometry and to the nature of precipitation, possible synergistic approaches are considered, to minimize the uncertainties of the different instruments, suggesting the blending of CML measurements with conventional precipitation estimates, such as rain gauges (Fencl et al., 2017; Haese et al., 2017), radar (Cummings et al., 2009; de Vos et al., 2019), or both (Grum et al., 2005; Bianchi et al., 2013).

If the general relationship between signal attenuation and rain rate is well established, with an obvious dependence on precipitation type and general climatological settings (e.g. air humidity), the success of the use of CML data to effectively monitor precipitation depends on the quality and general characteristics of the transmitted power data and on the fine tuning of the algorithms to the different physiography, climatic regimes and network topologies. The rather standardized policies of acquisition and storage of the different companies in different countries make the use of CMLs feasible all around the world, but there is no standard way yet to access them as scientific data. As they consist mostly of confidential maintenance data, major obstacles to face are the widespread unwillingness of releasing them cost-free and the bad data-quality standards (Chwala and Kunstmann, 2019).

https://doi.org/10.5194/amt-2020-43
Preprint. Discussion started: 27 February 2020


Atmospheric Measurement Techniques Discussions

The first objective of the present work is to make a validation of precipitation amounts and distributions estimated only from CML attenuation data, by means of a well established algorithm (i.e. RAINLINK, Overeem et al. (2016a)), over two areas of interest in the Po Valley (provinces of Bologna and Parma), where CML data have been obtained from Vodafone (direct purchase). Both areas contain river basins of considerable local interest, which will be addressed specifically. The further aim of the validation study is to set the background for a possible inclusion of CML data in the operational routine procedures for precipitation monitoring in the Meteorological Service of the Regional Agency for Environmental Protection and Energy (Arpae-SIMC).

In Section 2 we will describe the area of interest and the different rainfall datasets (CML, radar and rain gauges), including data quality and coverage. In Section 3 we will briefly describe the RAINLINK algorithm and the minor modifications performed to adapt it to the Emilia-Romagna area. The comparison – at single link and gridded map scales – between the rainfall estimates from the different data sources is presented and discussed in Section 4, while conclusions are provided in Section 5.

2 Data

We have considered a period of 57 days from 5 May to 30 June 2016. The two target areas for which we have available CML data are the provinces of Bologna (BO, 3702 km^2) and Parma (PR, 3447 km^2), both in the Po Valley in Emilia-Romagna, northern Italy (coloured areas in Figure 1). The physiography of the two regions is similar: the highest peaks (about 1,500 m a.s.l.) are located on the southern border, in the Apennine chain, while the central and northern part of the two areas are flat land. The two river basins (thick lines in Figure 1) are both located in the hilly part and have their closing sections located near the cities, in densely populated and assets-rich areas.

Precipitation climatology in the Po Valley during late spring season is characterized by both stratified structures and small scale convection, with highest rainfall amounts located in the hilly part. We divided the whole area into square boxes of $5\mathrm{km}\times5\mathrm{km}$ (see also Section 2.2.2) and this grid will be used to carry out rainfall interpolation and products intercomparison.

The validation has been carried out comparing, at different spatial and temporal scales, the rain amount obtained by CMLs, through the RAINLINK algorithm (Overeem et al., 2016a) with other rainfall estimates operationally available over the target domain. In particular, CML product has been compared with radar surface rain rates, both raw and gauge-corrected, rain gauges measurements and the operational precipitation analysis (ERG5) made available by Arpae-SIMC.

2.1 CMLs

Microwave attenuation data and metadata were purchased as a single dataset of two months, from Vodafone Italia S.p.A. within the Life EU project called RainBO LIFE15 CCA/IT/000035 (Alberoni et al., 2018). Received powers are measured by the provider at a frequency of ten times per second for maintenance purposes, but only maxima (P_{max}) and minima (P_{min}) readings in a 15 minutes time window are stored for backup. Therefore, data is in the format of 15 minutes $[P_{min}, P_{max}]$ pairs. All the available 357 CMLs are "duplex" links, so that two sub-links (back and forth) are present for the same link (although not always simultaneously active). Signal polarization is vertical for 259 CMLs, horizontal for the remaining 98, while carrier-

https://doi.org/10.5194/amt-2020-43
Preprint. Discussion started: 27 February 2020


Atmospheric Measurement Techniques Discussions

signal frequencies span from 6 to 42.6 GHz, with an average frequency ($\overline{f}$) of 22.1 GHz. Sublinks of the same CML share always the same polarization and differ only in frequency by a small gap of around one GHz. Path lengths of the links varies from 162 m to 30 km, the interquartile range extends between 2.4 and 8 km and the average length (LL) is 6 km. As expected, carrier frequency is anti-correlated with path length since high frequencies, while allowing a wider transmission band, are more subject to attenuation compared to the lower frequencies (Leijnse et al., 2008).

2.1.1 Coverage and data quality

The number of working CMLs varies slightly across the months: it grows from 348 at the beginning of May to the maximum of 357 in June. The number of valid CMLs for rain retrieval is lower because of the quality filtering performed by the pre-processor of the algorithm (see Section 3.1), resulting in an average number of 319 valid CMLs almost constant in time. Most of the rejected data is empty or incomplete (P_{min} or P_{max} missing), probably due to failures in reading or storing raw data.

Four parameters are utilized to summarize the topological structure of the CML network: the link density LD (defined as the total number of link paths divided by the total area, in km^{-2}), the average link length LL (in km), the bulk link coverage BC (defined as the sum of the link path lengths divided by the total area, in $\mathrm{km\ km}^{-2}$) and the local link coverage LC (calculated as BC but for each gridbox, in $\mathrm{km\ km}^{-2}$). Due to Vodafone confidentiality restrictions, we are not allowed to show the exact location of the available links, so we show instead in Figure 1 the spatial distribution of LC.

Since the RAINLINK original settings depend on the network characteristics, we compared the Emilia-Romagna network (ER) with the one from The Netherlands (NL), which is included in the RAINLINK software package as test sample (Overeem et al., 2016a), and with other datasets on which the algorithm was employed (Overeem et al., 2013, 2016b). The datasets properties are summarized and compared in Table 1. ER has comparable link density and higher average link length, resulting in a higher bulk coverage with respect to the NL network. The province of Bologna hosts more than half of the links (211 against 146) and thus has a higher LD.

2.1.2 Transmitting power levels

All the links are equipped with an Adaptive Transmission Power Control device (ATPC) which adapts the transmitting powers to the environmental conditions, in order to guarantee a minimum receiving power level at the other end of the link. This means that attenuation measurements should not be possible without knowing the transmitting powers too. That information is unfortunately not available to us again for confidentiality issues. To preserve the retrieval capabilities, data were corrected by the mobile operator itself, subtracting to the receiving powers the actual shift applied to the transmitting levels, thus simulating CML data with constant transmitting powers and so matching RAINLINK requirements.

https://doi.org/10.5194/amt-2020-43
Preprint. Discussion started: 27 February 2020


Atmospheric Measurement Techniques Discussions

2.2 Reference rainrate fields

2.2.1 Rain gauges

Rain gauges hourly data are provided by Arpae Rirer (regional hydro-meteorological network), established in 2001 by bringing together existing hydrological and meteorological station networks, managed at the time by various public bodies and regional authorities. The network of the whole Region is composed of 285 stations, equipped with tipping bucket rain gauges: 110 of them are divided in the Bologna (54) and Parma (56) provinces. Rain gauges have different sampling intervals (from 10 to 60 minutes), they undergo a process of homogenization and quality control and are released as hourly point-like product.

2.2.2 ERG5 rainfall analysis

The ERG5 gridded meteorological data set has been developed by Arpae-SIMC, in order to support agricultural activities in the region of Emilia-Romagna. ERG5 data are operationally produced since 2001, interpolating the hourly station measurements of the main meteorological variables (air temperature, relative humidity, precipitation, wind, solar irradiance) onto a $5\mathrm{km}\times5\mathrm{km}$ grid covering the Emilia-Romagna region. The interpolation method used for hourly precipitation consists of a Shepard (1968) modified scheme using topographic distances instead of Cartesian distances. This allows the interpolation to take into account the influence of topography on precipitation, by making locations separated by orographic obstacles more distant than they would be if Cartesian distances were used (Antolini et al., 2016). Data are stored and distributed freely in the form of GRIB2 files, which were imported in an R environment thanks to the rNOMADS package (Bowman and Lees, 2015). Among all the variables included in ERG5, we consider here only the hourly accumulated precipitation. Its input is based on the same Rirer network described in the previous Section, no longer limited to the two areas of study, but extended to the whole Region. Some discrepancies are therefore expected between the two products, mainly near the borders and in areas where the distribution of the instruments is less uniform.

2.2.3 Radars

Radar data set is based on hourly precipitation estimates obtained from the composite of the regional radar network managed by Arpae-SIMC. The regional network is composed by two C-Band systems, located in San Pietro Capofiume and in Gattatico (eastmost and westmost red crosses in Figure 1, respectively). For each instrument the equivalent radar reflectivity factor close to the ground is extracted and interpolated from polar coordinates to a 256×256 Cartesian grid of $1\mathrm{km}\times1\mathrm{km}$ resolution, then merged to obtain a composite of both radars.

Raw radar images are affected by various non-meteorological echoes that are removed before computing the Quantitative Precipitation Estimation (QPE). The current scheme used at Arpae-SIMC during operational service includes many steps: the ground clutter is removed at first statically through map of signal-free elevations recorded in dry conditions, then dynamically by combining a beam trajectory simulation at the current atmospheric state (as measured by radio soundings) and a Digital Elevation Model (Fornasiero et al., 2006). The beam blocking reduction and correction is performed based on a geometric optic

https://doi.org/10.5194/amt-2020-43
Preprint. Discussion started: 27 February 2020


Atmospheric Measurement Techniques Discussions

approach (Bech et al., 2003), while anomalous propagation is detected after the analysis of the echo coherence in the vertical direction (Alberoni et al., 2001). The final conversion between reflectivity and rainfall rate is performed on the corrected data set using the classic relationship $Z = aR^b$, with $a = 200$ and $b = 1.6$.

Rain rates are obtained every 5 minutes and the final rain total over a one-hour period is computed by an advection algorithm which takes into account the movement of the precipitating systems. The algorithm is based on the computation of maximum cross-correlation between consecutive maps, leading to the estimate of the displacement vector for each precipitating system. The rainfall field is then reconstructed every minute between the observations and cumulated over each hour. Finally, radar QPE is adjusted with rain gauges data, via the spatial analysis of the ratio G/R between rain gauges (G) and radar (R) rainfall rates over the station locations. The spatial analysis is obtained as weighted mean of the G/R values where the weight is a function of both the distance of the grid point from the station and the mean spacing between 5 observations (Koistinen and Puhakka, 1981; Amorati et al., 2012). In this work we will compare the CML product with both adjusted and unadjusted radar QPEs.

3 Methodology

The process chain which takes CML signals and returns rainfall maps is governed by the RAINLINK algorithm (Overeem et al., 2016a) published open source on GitHub (https://github.com/overeem11/RAINLINK) as an R package. We used the 1.14 version of the RAINLINK algorithm, available online from July 2019, and we added some minor modifications and optimizations (forked version available here: https://github.com/giacom0rovers1/RAINLINK).

3.1 CML rain retrieval algorithm

The algorithm works for both instantaneous power measurements and $[P_{min}, P_{max}]$ pairs: for the present work we use the latter, on 15 minutes intervals. The algorithm treats P_{min} and P_{max} separately (we will then use P_i to refer to both alternatively). Two separate rain estimates R_{min} and R_{max} will thus be obtained. The retrieval process works as follows:

1. **Preprocessing**: the raw input goes through a set of consistency checks to invalidate incomplete, wrongly identified or missing data.

2. **Wet-Dry Classification**: the samples are discriminated in wet and dry periods through the the so-called Nearby Links Approach (NLA): for each link, a time interval with a decrease in the received power is labelled as wet if at least half of the links in the vicinity (within 15 km radius) experience a comparable decrease. This is the second most computationally time-consuming step of the algorithm.

3. **Baseline determination**: a 24 h moving-window median of the quantity $\frac{1}{2}(P_{min} + P_{max})$ over the dry time intervals defines a reference level P_{ref} (baseline). This is the computationally heaviest operation of the algorithm.

https://doi.org/10.5194/amt-2020-43
Preprint. Discussion started: 27 February 2020


Atmospheric Measurement Techniques Discussions

4. **Outliers filter and power correction**: the information acquired in the two previous steps is used to remove outliers (through a fixed threshold) and noise. The corrected signal P_i^{Cor} will coincide to P_{ref} on dry periods and to P_i on wet ones.

5. **Rainrate retrieval**: attenuation A_i is computed as $A_i = P_{ref} - P_i^{Cor}$. A fixed quantity $Aa = 2.3$ dBm is subtracted from the attenuation A_i in order to take into account the wet-antenna effect, which is independent on path length and it is assumed independent also on frequency and rain intensity. If $A_i - Aa > 0$ then the specific attenuation k_i (dBm km^{-1}) is calculated as $k_i = (A_i - Aa)/L$, otherwise 0 is returned. Path-averaged mean rain intensities R_i (mm h^{-1}) are finally calculated using the $k - R$ relationship $R_i = a\,(k_i)^b$, where the coefficients a and b vary according to the frequency, polarization and drop size distribution (van Leth et al., 2018).

6. **Path-averaged rainfall depth**: to obtain a single path averaged rain depth, R_i are combined through a weighted mean: $R = \frac{1}{4}\left[\alpha R_{min} + (1-\alpha)\,R_{max}\right]$. The factor $\frac{1}{4}$ transforms rain rates in 15 min rain depths. The weight α varies between 0 (estimate derived from P_{max} only) and 1 (estimate derived from P_{min} only); we adopted the default value ($\alpha = 0.33$). We specify that, unlike Overeem et al. (2016a), we chose to keep the subscripts related to the original receiving powers, thus in our notation the rainrate R_{min} is greater than R_{max} because it is obtained from the most attenuated signal P_{min}.

7. **Interpolation**: interpolation is performed on a hourly scale (cumulated path-averaged rainfall depths) on the ERG5 grid with an ordinary kriging with a spherical isotropic variogram, whose parameters (NUGGET, SILL and RANGE) were defined by a two-year regional climatology.

3.2 RAINLINK implementation in northern Italy

The implementation of RAINLINK required some technical and conceptual considerations. The main differences between Italian and Dutch case studies concern links length, links frequency and orography. Our CMLs' operational frequencies span over a wider range than The Netherlands' ones, so the default frequency allowance window was extended from 12.5 - 40.5 GHz to 5.0 - 45.0 GHz in order not to miss any available information.

The NLA radius has to be consistent with the typical spatial correlation of rainfall and with the density of links available. In our case, the link density (0.045) is slightly higher than the one used for the original setup of the algorithm (0.043, see Table 1), and the spatial pattern of precipitation is expected to be similar in Italian and Dutch sites (Caracciolo et al., 2006). So, we let the settings for the wet-dry classification unaltered. Similarly, the k-R relationship is maintained, because northern Italy and Netherlands share similar climates and overall differences in drop size distributions between the two countries are expected to be negligible (Caracciolo et al., 2006) and certainly lower than variations of the same distribution along the link path and during the 15 minutes time intervals (Tokay et al., 2017).

3.3 Error metrics

In the present work we selected two sets of classical skill indicators, broadly used in the validation community (Puca et al., 2014), the first to assess the capability of the product to delineate rainfall occurrence (categorical indicators), and the second to

https://doi.org/10.5194/amt-2020-43
Preprint. Discussion started: 27 February 2020


Atmospheric Measurement Techniques Discussions

evaluate the skill in estimate correctly the quantitative precipitation rate (continuous indicators). The first set includes Probability of Detection (POD), False Alarm Ratio (FAR), Equitable Threat Score (ETS), and Multiplicative Bias (MB), while belong to the second set Normalized Mean Error (ME), Normalized Mean Absolute Error (MAE), Coefficient of Variation (CV), and the Pearsons' Correlation Coefficient (CC) (Nurmi, 2003; Overeem et al., 2016b).

Due to both interpolation and retrieval methodology, the CML precipitation rate and most of the reference fields we have used here can reach positive values that are sometimes very low and have no interest for any application, but which are potentially very influential in normalized error metrics. Thus we have set a wet-dry threshold equal to the minimum rain quantity detected by the tipping bucket rain gauge, i.e. 0.1 $\mathrm{mm\ h^{-1}}$. Categorical indicators are calculated with respect to this threshold for the whole dataset, while all the continuous indicators are computed only for the product-reference pairs where both values exceed the threshold (i.e. wet-wet). ME, MAE and CV are normalized with the averaged reference rain depth.

4 Comparison between CML and conventional precipitation products

We carried out the validation of CML product at three different levels. First, we compared single link estimates with the measurements of a nearby rain gauge, at the shortest temporal scale (15 minutes), to discuss success and failure cases, trying to understand the latter. Secondly, we compared the interpolated $5\mathrm{km}\times5\mathrm{km}$ CML hourly rainfall maps versus the ERG5 product at grid box scale. In the third step, the map comparison is carried out at basin scale including also the other precipitation products available at Arpae-SIMC.

4.1 Single link verification

We have selected links with an active rain gauge at a distance of at least an order of magnitude lower than the length of the link. They have been chosen in areas with different terrain and network density and far from the cities, as CMLs in urban areas are already well studied and also the most eligible to be replaced by optic fibers. Selected links had to be active for all the analysed period. In many cases more than one link was selected for one rain gauge. Temporal sampling is kept at the highest frequency, which is a measurement every 15 minutes for both the CML and the rain gauges. 12 rain gauges and 28 CMLs have been selected, 14 of which are in the northern part of the domain and the other 14 on the hilly region at elevations between 193 m and 960 m a.s.l..

The rain depths of the 28 CMLs are reported in Figure 2 for the whole study period, grouped accordingly to the closest rain gauge and ranked by its altitude. As a general comment, a large variability is found (ranging from near perfect agreement to discrepancy of a factor of 2 or 3 in the worst cases). Nonetheless, CC for the 28 links are between 0.67 and 0.86, proving an acceptable overall skill. In most cases, CMLs underestimate the rain gauge values: the links located in the lowlands (Figure 2a, 2b, 2d and 2e) show a better correspondence than those in the hilly regions, where underestimation is larger.

In some cases (Figure 2f, 2k and 2l) the discrepancies between CMLs of the same group but different in location, frequency and length are low compared to the discrepancies between each of them and the respective rain gauge: all these CMLs are in good mutual agreement and share the same classification issues, resulting in a systematic underestimation which therefore

https://doi.org/10.5194/amt-2020-43
Preprint. Discussion started: 27 February 2020


Atmospheric Measurement Techniques Discussions

seems to be caused by the algorithm setup. In other cases (Figure 2b, 2d and 2g) some links clearly outperforms others members of the same group. This second kind of discrepancies are more likely related to real differences like inhomogeneous rainy structures which crossed the link paths or different hardware setups (we do not know antennas specifications), while there is no evidence of a correlation with frequency or path length. In rare cases the disagreement takes place even between the two directions of the same link.

To gain a deeper understanding of better and worse performances of the single links, we performed some more detailed analysis on case studies at the rain-event scale (Figure 3). We show a case when the link retrievals properly match the measurements of the close-by raingauge, a case with markedly low performance, and lastly a case that shows the impact of a well know problem in any microwave-based precipitation retrieval: the melting layer. In Figure 3 graph panels are organized in columns by CML and in rows by sub-link. In the top panel rain gauge measurements (blue dots) are compared with CML estimates (purple line) and also the minimum and maximum attenuation signals are plotted (A_{max} and A_{min} respectively). The grey background indicates when the classification detects a dry period. The pink background indicates the band inside which attenuation is considered as caused by a wet antenna (Aa parameter) and is discarded for rain retrieval. In the middle panel all the signals managed by the algorithm are shown: the reference power P_{ref}, the raw received powers P_{min} and P_{max} and the filtered received powers P_{min}^{Cor} and P_{max}^{Cor}. The bottom panel shows the cumulated rainfall depth in the same time frame.

4.1.1 Best cases example

Between 11 and 12 May 2016 the NLA classification on the three links near Sant'Agata (Bologna, 18 m a.s.l.) works properly: in Figure 3a most blue dots (rain gauge measurements) are on white background. In Figure 3d, after the attenuation event, the noisy signal is correctly filtered and a very small amount of rain (just above the gauge threshold) is neglected. The agreement is qualitatively very high between each pair of sub-links and good among the different links, in terms of specific attenuations and retrieved quantities. Quantitative retrievals give some overestimation for one of the CMLs, whose effect is evident on the accumulation plot (Figure 3g) where the total rain depths are compared. During the two months the Sant'Agata links are generally in good agreement with the close-by rain gauge, with CC ranging between 0.61 and 0.86 and CV between 0.4 and 0.7.

4.1.2 Worst cases example

On Vergato (193 m a.s.l.) between 8 and 10 June 2016 many events are missed due to wet-dry misclassification (Figure 3b) which result in a 20 mm loss in the rain accumulation (Figure 3h). Looking at Figure 3e P_{min} (orange) does in fact sense the missed rainfalls, but P_{max} (blue) does not. This suggests that there are power fluctuations which develop and completely end during a single time interval of 15 min. This high variability could prevent the NLA to see the required spatial correlation to identify wet periods. The POD over the whole period for these two links is between 0.34 and 0.36.

When the NLA classification works correctly, there is still a general quantitative underestimation. It could be seen that half of the signal is hidden from the wet antenna attenuation threshold: in this case we can suggest that the antenna could be dry, due to wind or no rain directly on it, so the Aa threshold is too high (also noted by de Vos et al. (2019)). The continuous scores

https://doi.org/10.5194/amt-2020-43
Preprint. Discussion started: 27 February 2020


Atmospheric Measurement Techniques Discussions

for the wet-wet sample on the whole period show a good correlation with gauges but are poor in statistical relevance because of the high number of misses. They nevertheless confirm the tendency to quantitatively underestimate, by around 20%.

For this pair of links located in the hilly Reno river basin there is therefore both a (minor) issue in quantitative underestimation and a (major) issue in the detection capability of the NLA classification.

4.1.3 Melting layer case

The presence of melting layer is a critical issue in retrieving precipitation at the ground by microwave signal (i.e. radar sensors), so we take advantage of a winter time subset of data obtained from Vodafone for testing, but not numerous enough to perform a systematic analysis.

When the melting layer of a precipitating cloud crosses the link path (e.g. the antennas are on two hill crests and the link goes a few hundred meters high above the valley) the attenuation signal grows abruptly and leads to widespread overestimation. In Figures 3c, 3f, 3i we see it happening over Vergato on 3 March 2016. One of the two CMLs close to Vergato station has no estimates (it was probably rejected by the algorithm during initial filtering) but the signal is evident nonetheless.

This issue could be mitigated via the joint use of radar and CML measurements: the melting layer which produces strong attenuation is the same that causes the "bright band" in the radar reflectivity maps and is thus easily detected.

4.2 Gridded product verification

The verification of the RAINLINK gridded product ($1\ \mathrm{h}$ cumulated on the $5\mathrm{km}\times5\mathrm{km}$ grid) with respect to the ERG5 product is first performed at the highest available resolution, therefore grid box by grid box, since the two products intentionally share the same interpolation grid. Secondly, the comparison is carried out at the basin-scale by matching spatially averaged time series over areas of different size, in parallel with other operational precipitation products available at Arpae-SIMC.

4.2.1 Highest resoluton matching

Figure 4 shows a scatter density plot for the whole dataset over the entire period. CML estimates from RAINLINK in northern Italy over uneven ground have an overall underestimating performance of -26$\%$ on the accumulated rain over the two months. The CV is 0.77 and R^2 (the square of the already defined Pearson's correlation coefficient CC) is 0.47, based on a sample of 10638 total wet hours. These performances are in good agreement with similar studies (Overeem et al., 2013, 2016b) despite the differences in the products involved: comparison between our results and the ones presented in the mentioned works are shown in Table 2.

As mentioned, the data set was filtered so that only the rainfall depths of the grid boxes in which both CMLs and ERG5 reported more than $0.1\ \mathrm{mm}$ were used for the quantitative indicators. The performances of the rain detection capabilities with respect to this threshold are evaluated separately with the already presented categorical scores (see Section 3.3).

The means of categorical and continuous indicators are computed on five areas, with different extension (S) and averaged Link Coverage ($\overline{LC}$), and reported in Table 3, ranked according to the $\overline{LC}$ value: Parma Province (PP), Total Area (TA), Parma

https://doi.org/10.5194/amt-2020-43
Preprint. Discussion started: 27 February 2020


Atmospheric Measurement Techniques Discussions

river Basin (PRB), Bologna Province (BP), Reno River Basin (RRB). The total area and the two provinces do not have any specific hydrological meaning, but could be seen as a good foretype of larger river basins with heterogeneous terrain (see Figure 1). All normalized indicators are relative to the average reference (ERG5) rain rate. Numbers in bold (italics) are the best (worst) value in the column.

The general tendency of the RAINLINK product is confirmed also for the sub-areas (excluding RRB for now) to underestimate the rain occurrence (MB < 1), with a relatively low value of POD (0.48 to 0.57) in all areas. The FAR is also rather low, (0.28 to 0.32), resulting in ETS values (0.38 to 0.43) comparable to the values obtained in the validation of other precipitation estimates, e.g. as the ones available from satellite observations (Puca et al., 2014; Feidas et al., 2018). Mean Error confirms the underestimation of rain amount (ME between -0.19 and -0.34), CV ranges between 0.73 and 0.80, CC between 0.62 and 0.74.

The averages over the Reno River Basin stand out for all the indicators, either positively or negatively, therefore they need a separate discussion. As highlighted in Table 3 by bold and italics fonts, RRB has half the FAR the other samples have (0.16), almost ten points less CV (0.63) and almost fifteen points better CC (0.8, which is unexpectedly high), with the mean errors aligned to the other samples. The accuracy in the estimates is reached at the expense of POD, ETS and BIAS: around 50% of the rainfall duration is lost in this area. The main peculiarity of the RRB area is the high $\overline{LC}$, which is 50% higher than the rest of the field. We can infer that the higher coverage led, via the nearby links approach, to a very strict classification, which reduced FAR and produced some misses. This is in agreement with what is seen in the single link analysis of the Vergato CMLs (Section 4.1.2), which are located inside the Reno river basin.

Since a sensitivity to LC seems likely, we further investigate its effect on scores by grouping each grid box by LC quartiles, regardless of the actual geographical location, and reported the results in Figure 5. For four out of six indicators improve as LC increases (FAR, ETS, CC and CV) the most striking is the FAR, as it had already been noticed in the case of the Reno river basin. The POD remains mostly unchanged, therefore the ETS improves only slightly, but we do not, however, see the POD sharp decline that occurred in the Reno basin: this suggests that LC is probably not the only variable at play there. Other studies will be conducted in the future to better investigate these problems, as well as a local calibration of the algorithm parameters (e.g. Aa and α).

The values presented above are fully comparable, and in many cases better, than the ones obtained for the main satellite based rainfall products in similar regions. Petracca et al. (2018) analysed over Italy the instantaneous estimate of the Global Precipitation Measurement - Dual-frequency Precipitation Radar (GPM-DPR), considered as the most reliable and accurate instrument to measure precipitation from space. Over a footprint of size comparable to the one used in this paper, the best value of CC is 0.57, while the CV was between 1 and 2. Other validation studies of GPM-DPR products in the alpine region (Speirs et al., 2017) obtained relatively good POD (up to 0.78), FAR (below 0.08) and CC (up to 0.63) over flat terrain, with dramatic drop of the skill indicators when areas with complex topography is considered.

4.2.2 Area-average matching

In this Section the matching between estimate and reference field is performed at basin (and Province) scales, comparing hourly rain amounts averaged over areas of different sizes. The areas selected for this evaluation are the ones introduced in the

https://doi.org/10.5194/amt-2020-43
Preprint. Discussion started: 27 February 2020


Atmospheric Measurement Techniques Discussions

previous Section: two of them are selected because of direct hydrological interest (RRB and PRB), while the other three (BP, PP and TA) are chosen to assess the impact of increasing target area.

The categorical (rain/no-rain 0.1 $\mathrm{mm\,h^{-1}}$ threshold) and continuous (on wet-wet occurrences) indicators for the five mentioned areas are reported in Table 4, listed this time in order of increasing area size. In general, best performances are found for the largest areas (BP and TA), while the smallest ones (PRB and RRB) show the worst values. CML product underestimate precipitation occurrence (MB between 0.41 and 0.70) and amount (ME between -0.23 and -0.43) at all scales. Due to the areal averaging, CC is markedly higher than the high-resolution values reported in Table 3. The characteristic behaviour of RRB (lowest FAR and POD, highest CC) remains also in this case.

The same areal-averaged statistical indicators have been computed also for the operational products available at Arpae-SIMC for operational use and described in Section 2.2, all reported to a hourly scale and compared with the ERG5 product. We show in Figure 6 the values of the statistical indicators as function of the target area.

The raingauge product, obtained by averaging the measurements of the raingauges in the area, performs similarly to its interpolated version ERG5, as expected, and diverges only for small areas, where the impact of a single sensor in disagreement with neighbours is the highest.

Radar product shows, in this metric, almost the same performance with or without the gauge adjustment. Both have very good detection capabilities (POD is almost 1) but high rates of false alarms (FAR around 0.5) and marked quantitative discrepancies (MAE around 1, CV between 1.5 and 2). Radar however can see finer precipitation structure given its spatially continuous coverage, while rain gauge and CML networks (with point-like and line-integrated observations), are both prone to miss some information from small scale events, often observed between meteorological spring and summer in Italy.

The CML product outperforms both radar products in terms of CC, CV, MAE and FAR, while it clearly lacks in detection capability (CMLs POD between 0.4 and 0.6), as discussed in the previous Section. CML retrieval process, being based on electromagnetic attenuation instead of back-scattering, does not share the radar's high sensitivity to the size distribution of the hydrometeors (Leijnse et al., 2008), thus making CML a more robust sensor. Figure 7 shows the overestimating behaviour of both radar products and the average underestimation of the CML product. The spread is more relevant for radars than CML, but the latter has a smaller sample size due to the already mentioned low POD issues.

In an operational context, it is of great relevance the latency of the precipitation product, i.e. the time taken from the acquisition of the basic data (the occurrence of the event) and the delivery of the product in a ready-to-use form. In Table 5 are reported the latency and sampling characteristics of the four precipitation products we took for comparison, along with CML product. CMLs operational specifications refer to an implementation of the RAINLINK algorithm as part of a real-time service, tested in 2019 by MEEO S.r.l. within the RainBO project (LIFE15 CCA/IT/000035). It can be seen that the combination of short latency and good coverage provided by CMLs is unmatched by all products except the raw radar, which though lacks the required quantitative accuracy.

https://doi.org/10.5194/amt-2020-43
Preprint. Discussion started: 27 February 2020


Atmospheric Measurement Techniques Discussions

5 Conclusions

An assessment of the rainfall retrieval capability of CML opportunistic sensors over heterogeneous terrain in northern Italy is conducted at various levels for two months of data. First, a sample of 28 CMLs (out of the total 319) is compared with the closest raingauge at a 15 min scale. Overestimation and underestimation of rain amount are both present, though the latter appears dominant, with a marked variability among different links, with a generally acceptable skill (CC from 0.67 to 0.86). Higher elevation CMLs show in general worst performances, being also prone to known shortcomings, such as melting layer across the microwave path, which led to significant performance drops.

Interpolated products obtained from the full sample of 319 links confirm that a non-negligible quantity of rain is missed (normalized Mean Error is -0.26, overall CC is 0.68 and overall CV is 0.77), but also show that the rain detection capability is suitable for operational application, especially if integrated over large areas (CC rises to 0.92). Negative impact on the overall results comes from areas with poor sensor coverage (i.e. low density of link), especially in terms of increased false alarms. The results show a high variability of responses, with an overall skill in agreement with other CML studies.

Furthermore, the validation scheme implemented for this work, if a more complete dataset would become available, would be used to improve the performance of RAINLINK by tuning the algorithm parameters (NLA radius, Aa, α) on a more complete training sample specific of the study area.

Finally, when compared to other products currently available for operational real-time exploitation, CML sensors show similar or better abilities than their counterparts, especially if latency is also taken into account. Hence an integration of microwave links sensors in an operational service is highly desirable.

Code and data availability. CML data were provided by Vodafone Italia S.p.A.. via direct purchase from MEEO S.r.l. and are not publicly available. Gauge data from Emilia-Romagna are freely available at https://simc.arpae.it/dext3r/. Radar reflectivities in near real-time are freely available at https://www.arpae.it/sim/?osservazioni_e_dati/radar, while derived rain products and ERG5 analyses are available upon request at Arpae-SIMC (https://www.arpae.it/sim/). The core algorithm is available (open source) at https://github.com/giacom0rovers1/RAINLINK and was forked from https://github.com/overeem11/RAINLINK on the 26th of August 2019 (RAINLINK version 1.14).

Author contributions. GR adapted the RAINLINK code to Italian data, ran the analysis, plotted the data and contributed to the interpretation of the results and to the writing of the manuscript. PPA and AF performed the reference data pre-processing and contributed to data analysis. FP contributed to the design of the validation strategy, to the interpretation of the results and to the writing of the paper.

Competing interests. The Author declare that no competing interests are present.

https://doi.org/10.5194/amt-2020-43
Preprint. Discussion started: 27 February 2020

Atmospheric Measurement Techniques Discussions

Acknowledgements. This work has been partially funded by the Life EU Project RainBO (LIFE15 CCA/IT/000035). The Authors thank Stefania Pasetti and Marco Folegani of MEEO S.r.l. (www.meeo.it) for their support, and are grateful to D. Vecchiato and A. Viaro of Vodafone Italia S.p.A. for the technical assistance with the data. We also thank Aart Overeem, for having developed and released open source the RAINLINK algorithm and for the kind feedback and support he provided to this research.

https://doi.org/10.5194/amt-2020-43
Preprint. Discussion started: 27 February 2020

Atmospheric Measurement Techniques Discussions

References

Abdulrahman, A., Bin Abdulrahman, T., Bin Abdulrahim, S., and Kesavan, U.: Comparison of measured rain attenuation and ITU-R predictions on experimental microwave links in Malaysia, International Journal of Microwave and Wireless Technologies, 3, 477–483, https://doi.org/10.1017/S1759078711000171, 2011.

Alberoni, P. P., Andersson, T., Mezzasalma, P., Michelson, D. B., and Nanni, S.: Use of the vertical reflectivity profile for identification of anomalous propagation, Meteorological Applications, 8, 257–266, https://doi.org/10.1017/S1350482701003012, 2001.

Alberoni, P. P., Fornasiero, A., Roversi, G., Pasetti, S., Folegani, M., and Porcù, F.: Comparison between different QPE based on: Microwave Links, Radar adjusted and Gauges, in: 10th European Conference on Radar in Meteorology and Hydrology, pp. 851–860, KNMI, https://doi.org/10.18174/454537, 2018.

Amorati, R., Alberoni, P., and Fornasiero, A.: Operational Bias Correction of Hourly Radar Precipitation Estimate using Rain Gauges, in: Proceedings of the Seventh Eropean Conference on Radar in meteorology and Hydrology, http://www.meteo.fr/cic/meetings/2012/ERAD/extended_abs/QPE_007_ext_abs.pdf, 2012.

Antolini, G., Auteri, L., Pavan, V., Tomei, F., Tomozeiu, R., and Marletto, V.: A daily high-resolution gridded climatic data set for Emilia Romagna, Italy, during 1961-2010, International Journal of Climatology, 36, 1970–1986, 2016.

Bech, J., Codina, B., Lorente, J., and Bebbington, D.: The Sensitivity of Single Polarization Weather Radar Beam Blockage Correction to Variability in the Vertical Refractivity Gradient, Journal of Atmospheric and Oceanic Technology, 20, 845–855, https://doi.org/10.1175/1520-0426(2003)020<0845:TSOSPW>2.0.CO;2, 2003.

Berne, A. and Uijlenhoet, R.: Path-averaged rainfall estimation using microwave links: Uncertainty due to spatial rainfall variability, Geophysical Research Letters, 34, https://doi.org/10.1029/2007GL029409, 2007.

Bianchi, B., Jan van Leeuwen, P., Hogan, R. J., and Berne, A.: A Variational Approach to Retrieve Rain Rate by Combining Information from Rain Gauges, Radars, and Microwave Links, Journal of Hydrometeorology, 14, 1897–1909, https://doi.org/10.1175/JHM-D-12-094.1, 2013.

Bowman, D. and Lees, J.: Near real time weather and ocean model data access with rNOMADS, Computers and Geosciences, 78, 88 – 95, https://doi.org/https://doi.org/10.1016/j.cageo.2015.02.013, 2015.

Caracciolo, C., Prodi, F., and Uijlenhoet, R.: Comparison between Pludix and impact/optical disdrometers during rainfall measurement campaigns, Atmospheric Research, 82, 137 – 163, https://doi.org/https://doi.org/10.1016/j.atmosres.2005.09.007, 14th International Conference on Clouds and Precipitation, 2006.

Chwala, C. and Kunstmann, H.: Commercial microwave link networks for rainfall observation: Assessment of the current status and future challenges, WIREs Water, 6, e1337, https://doi.org/10.1002/wat2.1337, 2019.

Cummings, R., Upton, G., Holt, A., and Kitchen, M.: Using microwave links to adjust the radar rainfall field, Advances in Water Resources, 32, 1003 – 1010, https://doi.org/https://doi.org/10.1016/j.advwatres.2008.08.010, weather Radar and Hydrology, 2009.

de Vos, L., Raupach, T., Leijnse, H., Overeem, A., Berne, A., and Uijlenhoet, R.: High-Resolution Simulation Study Exploring the Potential of Radars, Crowdsourced Personal Weather Stations, and Commercial Microwave Links to Monitor Small-Scale Urban Rainfall, Water Resources Research, 54, 10 293–10 312, https://doi.org/10.1029/2018WR023393, 2018.

de Vos, L. W., Overeem, A., Leijnse, H., and Uijlenhoet, R.: Rainfall Estimation Accuracy of a Nationwide Instantaneously Sampling Commercial Microwave Link Network: Error Dependency on Known Characteristics, Journal of Atmospheric and Oceanic Technology, 36, 1267–1283, https://doi.org/10.1175/JTECH-D-18-0197.1, 2019.

https://doi.org/10.5194/amt-2020-43
Preprint. Discussion started: 27 February 2020

Atmospheric Measurement Techniques Discussions

Doumounia, A., Gosset, M., Cazenave, F., Kacou, M., and Zougmore, F.: Rainfall monitoring based on microwave links from cellular telecommunication networks: First results from a West African test bed, Geophysical Research Letters, 41, 6015–6021, https://doi.org/10.1002/2014GL060724, 2014.

Feidas, H., Porcu, F., Puca, S., Rinollo, A., Lagouvardos, C., and Kotroni, V.: Validation of the H-SAF precipitation product H03 over Greece using rain gauge data, Theoretical and Applied Climatology, 131, 377–398, https://doi.org/10.1007/s00704-016-1981-9, 2018.

Fencl, M., Rieckermann, J., Schleiss, M., Stránský, D., and Bareš, V.: Assessing the potential of using telecommunication microwave links in urban drainage modelling, Water science and technology : a journal of the International Association on Water Pollution Research, 68, 1810–8, https://doi.org/10.2166/wst.2013.429, 2013.

Fencl, M., Dohnal, M., Rieckermann, J., and Bareš, V.: Gauge-adjusted rainfall estimates from commercial microwave links., Hydrology and Earth System Sciences, 21, 617–634, https://doi.org/https://doi.org/10.5194/hess-21-617-2017, 2017.

Fenicia, F., Pfister, L., Kavetski, D., Matgen, P., Iffly, J.-F., Hoffmann, L., and Uijlenhoet, R.: Microwave links for rainfall estimation in an urban environment: Insights from an experimental setup in Luxembourg-City, Journal of Hydrology, 464-465, 69 – 78, https://doi.org/https://doi.org/10.1016/j.jhydrol.2012.06.047, 2012.

Fornasiero, A., Bech, J., and Alberoni, P. P.: Enhanced radar precipitation estimates using a combined clutter and beam blockage correction technique, Natural Hazards Earth System Science, 6, 697–710, https://doi.org/10.5194/nhess-6-697-2006, 2006.

Grecu, M., Olson, W., Munchak, s., Ringerud, S., Liao, L., Haddad, Z., Kelley, B., and McLaughlin, S.: The GPM combined algorithm, Journal of Atmospheric and Oceanic Technology, 33, 2225–2245, https://doi.org/10.1175/JTECH-D-16-0019.1, 2016.

Grum, M., Kraemer, S., Verworn, H.-R., and Redder, A.: Combined use of point rain gauges, radar, microwave link and level measurements in urban hydrological modelling, Atmospheric Research, 77, 313 – 321, https://doi.org/https://doi.org/10.1016/j.atmosres.2004.10.013, precipitation in Urban Areas, 2005.

Haese, B., Hörning, S., Chwala, C., Bardossy, A., Schalge, B., , and Kunstmann, H.: Stochastic Reconstruction and Interpolation of Precipitation Fields Using Combined Information of Commercial Microwave Links and Rain Gauges, Water Resources Research, 53, 10 740–10 756, https://doi.org/https://doi.org/10.1002/2017WR021015, 2017.

Harden, B., Norbury, J., and White, W.: Attenuation/rain-rate relationships on terrestrial microwave links in the frequency range 10- -40 GHz, Electronics Letters, 14, 154 – 155, https://doi.org/10.1049/el:19780103, 1978.

Huuskonen, A., Saltikoff, E., and Holleman, I.: The Operational Weather Radar Network in Europe, Bulletin of the American Meteorological Society, 95, 897–907, https://doi.org/10.1175/BAMS-D-12-00216.1, 2014.

Jameson, A. R.: Estimating the Path-Average Rainwater Content and Updraft Speed along a Microwave Link, Journal of Atmospheric and Oceanic Technology, 10, 478–485, https://doi.org/10.1175/1520-0426(1993)010<0478:ETPARC>2.0.CO;2, 1993.

Koistinen, J. and Puhakka, T.: An improved spatial gauge-radar adjustment technique, in: Preprints of the 20th Conference on Radar Meteorology, p. 179–186, Am. Meteorol. Soc., 1981.

Lanza, L. and Stagi, L.: Non-parametric error distribution analysis from the laboratory calibration of various rainfall intensity gauges, Water science and technology : a journal of the International Association on Water Pollution Research, 65, 1745–52, https://doi.org/10.2166/wst.2012.075, 2012.

Leijnse, H., Uijlenhoet, R., and Stricker, J.: Microwave link rainfall estimation: Effects of link length and frequency, temporal sampling, power resolution, and wet antenna attenuation, Advances in Water Resources, 31, 1481–1493, https://doi.org/10.1016/j.advwatres.2008.03.004, 2008.

https://doi.org/10.5194/amt-2020-43
Preprint. Discussion started: 27 February 2020

Leijnse, H., Uijlenhoet, R., and Berne, A.: Errors and Uncertainties in Microwave Link Rainfall Estimation Explored Using Drop Size Measurements and High-Resolution Radar Data, Journal of Hydrometeorology, 11, 1330–1344, https://doi.org/10.1175/2010JHM1243.1, 2010.

Mugnai, A., Casella, D., Cattani, E., Dietrich, S., Laviola, S., Levizzani, V., Panegrossi, G., Petracca, M., Sanò, P., Di Paola, F., Biron, D., De Leonibus, L., Melfi, D., Rosci, P., Vocino, A., Zauli, F., Pagliara, P., Puca, S., Rinollo, A., Milani, L., Porcù, F., and Gattari, F.: Precipitation products from the hydrology SAF, Natural Hazards and Earth System Sciences, 13, 1959–1981, https://doi.org/10.5194/nhess-13-1959-2013, 2013.

Mulangu, C. and Afullo, T.: Variability of the propagation coefficients due to rain for microwave links in southern Africa, Radio Science - RADIO SCI, 44, https://doi.org/10.1029/2008RS003912, 2009.

Nurmi, P.: Recommendations on the verification of local weather forecasts, ECMWF Technical Memorandum, 430, 2003.

Overeem, A., Leijnse, H., and Uijlenhoet, R.: Measuring urban rainfall using microwave links from commercial cellular communication networks, Water Resources Research, 47, https://doi.org/10.1029/2010WR010350, 2011.

Overeem, A., Leijnse, H., and Uijlenhoet, R.: Country-wide rainfall maps from cellular communication networks, Proceedings of the National Academy of Sciences, 110, 2741–2745, https://doi.org/10.1073/pnas.1217961110, 2013.

Overeem, A., Leijnse, H., and Uijlenhoet, R.: Retrieval algorithm for rainfall mapping from microwave links in a cellular communication network, Atmospheric Measurement Techniques, 9, 2425–2444, https://doi.org/10.5194/amt-9-2425-2016, 2016a.

Overeem, A., Leijnse, H., and Uijlenhoet, R.: Retrieval algorithm for rainfall mapping from microwave links in a cellular communication network, Atmospheric Measurement Techniques, 9, 2425–2444, https://doi.org/10.5194/amt-9-2425-2016, 2016b.

Petracca, M., D'Adderio, L., Porcu, F., Vulpiani, G., Stefano, S., and Puca, S.: Validation of GPM Dual-Frequency Precipitation Radar (DPR) Rainfall Products over Italy, Journal of Hydrometeorology, 19, 907–925, https://doi.org/10.1175/JHM-D-17-0144.1, 2018.

Porcù, F., Milani, L., and Petracca, M.: On the uncertainties in validating satellite instantaneous rainfall estimates with raingauge operational network, Atmospheric Research, 144, 73–81, https://doi.org/10.1016/j.atmosres.2013.12.007, 2014.

Puca, S., Porcu, F., Rinollo, A., Vulpiani, G., Baguis, P., Balabanova, S., Campione, E., Erturk, A., Gabellani, S., Iwanski, R., Jurašek, M., Kaňák, J., Kerényi, J., Koshinchanov, G., Kozinarova, G., Krahe, P., Lapeta, B., Labo, E., Milani, L., and Gattari, F.: The validation service of the hydrological SAF geostationary and polar satellite precipitation products, Natural hazards and earth system sciences, 14, 871–889, https://doi.org/10.5194/nhess-14-871-2014, 2014.

Rahimi, A. R., Holt, A. R., Upton, G. J. G., and Cummings, R. J.: Use of dual-frequency microwave links for measuring path-averaged rainfall, Journal of Geophysical Research: Atmospheres, 108, https://doi.org/10.1029/2002JD003202, 2003.

Rincon, R. and Lang, R.: Microwave link dual-wavelength measurements of path-average attenuation for the estimation of drop size distributions and rainfall, Geoscience and Remote Sensing, IEEE Transactions on, 40, 760 – 770, https://doi.org/10.1109/TGRS.2002.1006324, 2002.

Rios Gaona, M., Overeem, A., Raupach, T., Leijnse, H., and Uijlenhoet, R.: Rainfall retrieval with commercial microwave links in São Paulo, Brazil, Atmospheric Measurement Techniques Discussions, pp. 1–21, https://doi.org/10.5194/amt-2017-287, 2017.

Ryzhkov, A. and Zrnic, D.: Radar Polarimetry for Weather Observations, Springer Atmospheric Sciences, https://doi.org/10.1007/978-3-030-05093-1, 2019.

Saltikoff, E., Haase, G., Delobbe, L., Gaussiat, N., Martet, M., Idziorek, D., Leijnse, H., Novák, P., Lukach, M., and Stephan, K.: OPERA the Radar Project, Atmosphere, 10, 320, https://doi.org/10.3390/atmos10060320, 2019.

https://doi.org/10.5194/amt-2020-43
Preprint. Discussion started: 27 February 2020

Serafin, R. J. and Wilson, J. W.: Operational Weather Radar in the United States: Progress and Opportunity, Bulletin of the American Meteorological Society, 81, 501–518, https://doi.org/10.1175/1520-0477(2000)081<0501:OWRITU>2.3.CO;2, 2000.

Shepard, D.: A Two-Dimensional Interpolation Function for Irregularly-Spaced Data, in: Proceedings of the 1968 23rd ACM National Conference, ACM '68, p. 517–524, Association for Computing Machinery, New York, NY, USA, https://doi.org/10.1145/800186.810616, 1968.

Skofronick-Jackson, G., Petersen, W. A., Berg, W., Kidd, C., Stocker, E. F., Kirschbaum, D. B., Kakar, R., Braun, S. A., Huffman, G. J., Iguchi, T., Kirstetter, P. E., Kummerow, C., Meneghini, R., Oki, R., Olson, W. S., Takayabu, Y. N., Furukawa, K., and Wilheit, T.: The Global Precipitation Measurement (GPM) Mission for Science and Society, Bulletin of the American Meteorological Society, 98, 1679–1695, https://doi.org/10.1175/BAMS-D-15-00306.1, 2017.

Speirs, P., Gabella, M., and Berne, A.: A comparison between the GPM dual-frequency precipitation radar and ground-based radar precipitation rate estimates in the Swiss Alps and Plateau, Journal of Hydrometeorology, 18, 1247–1269, https://doi.org/10.1175/JHM-D-16-0085.1, 2017.

Tan, M. L., Samat, N., Chan, N. W., and Roy, R.: Hydro-Meteorological Assessment of Three GPM Satellite Precipitation Products in the Kelantan River Basin, Malaysia, Remote Sensing, 10, 1011, https://doi.org/10.3390/rs10071011, 2018.

Tokay, A., D'Adderio, L. P., Porcù, F., Wolff, D. B., and Petersen, W. A.: A Field Study of Footprint-Scale Variability of Raindrop Size Distribution, Journal of Hydrometeorology, 18, 3165–3179, https://doi.org/10.1175/JHM-D-17-0003.1, 2017.

Turner, D. J. W. and Turner, D.: Attenuation due to rainfall on a 24 km microwave link working at 11, 18 and 36 GHz, Electronics Letters, 6, 297–298, https://doi.org/10.1049/el:19700208, 1970.

Upton, G., Holt, A., Cummings, R., Rahimi, A., and Goddard, J.: Microwave links: The future for urban rainfall measurement?, Atmospheric Research, 77, 300–312, https://doi.org/10.1016/j.atmosres.2004.10.009, 2005.

van Leth, T., Overeem, A., Leijnse, H., and Uijlenhoet, R.: A measurement campaign to assess sources of error in microwave link rainfall estimation, Atmospheric Measurement Techniques, 11, 4645–4669, https://doi.org/10.5194/amt-11-4645-2018, 2018.

van Leth, T. C., Leijnse, H., Overeem, A., and Uijlenhoet, R.: Estimating raindrop size distributions using microwave link measurements, Atmospheric Measurement Techniques Discussions, 2019, 1–27, https://doi.org/10.5194/amt-2019-51, 2019.

https://doi.org/10.5194/amt-2020-43
Preprint. Discussion started: 27 February 2020

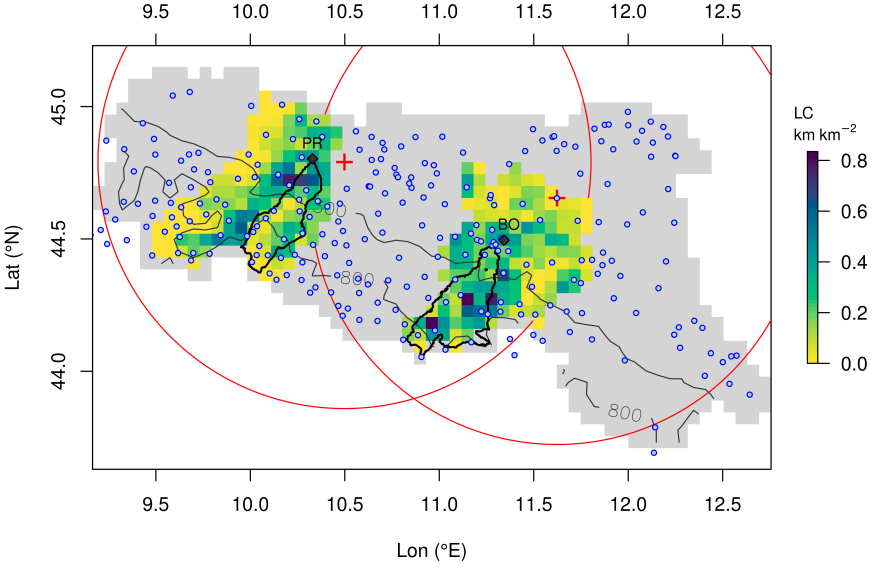

Figure 1. Map of the Emilia-Romagna region in Northern Italy (grey area). The coloured areas are the two Provinces where the CML estimates are computed (the color scale represents the Link Coverage, LC) and black thick lines delimit the two river basins (Parma, to the east, and Reno). Blue dots and red crosses indicate operational raingauge and weather radar locations, respectively, while red circles are the 100 km radar coverage. Thin black lines show two elevation contours (300 and 800 m a.s.l.). The main cities in the area Bologna and Parma are indicated with the black diamonds.

https://doi.org/10.5194/amt-2020-43
Preprint. Discussion started: 27 February 2020

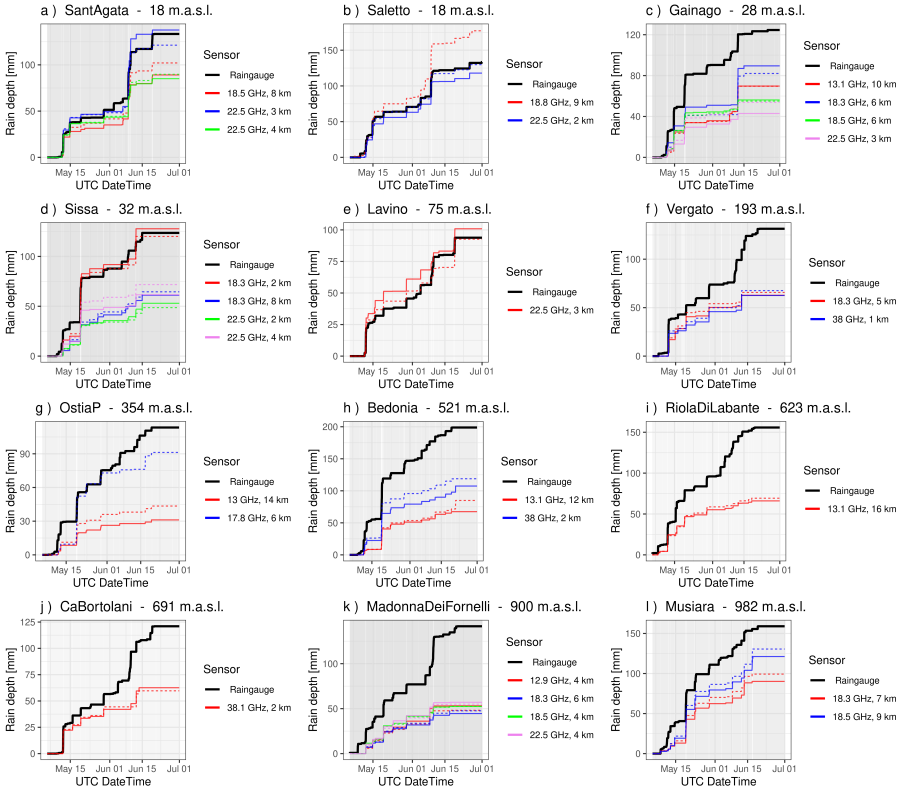

Figure 2. Accumulated rain depths over the whole period for the 28 CMLs selected for the single-link analysis. Each tile is named by the corresponding rain gauge, whose accumulated rain depth is shown by the black thick line. Solid and dashed lines represent the two directions (if both active) for every CML (distinguished by colour).

https://doi.org/10.5194/amt-2020-43
Preprint. Discussion started: 27 February 2020

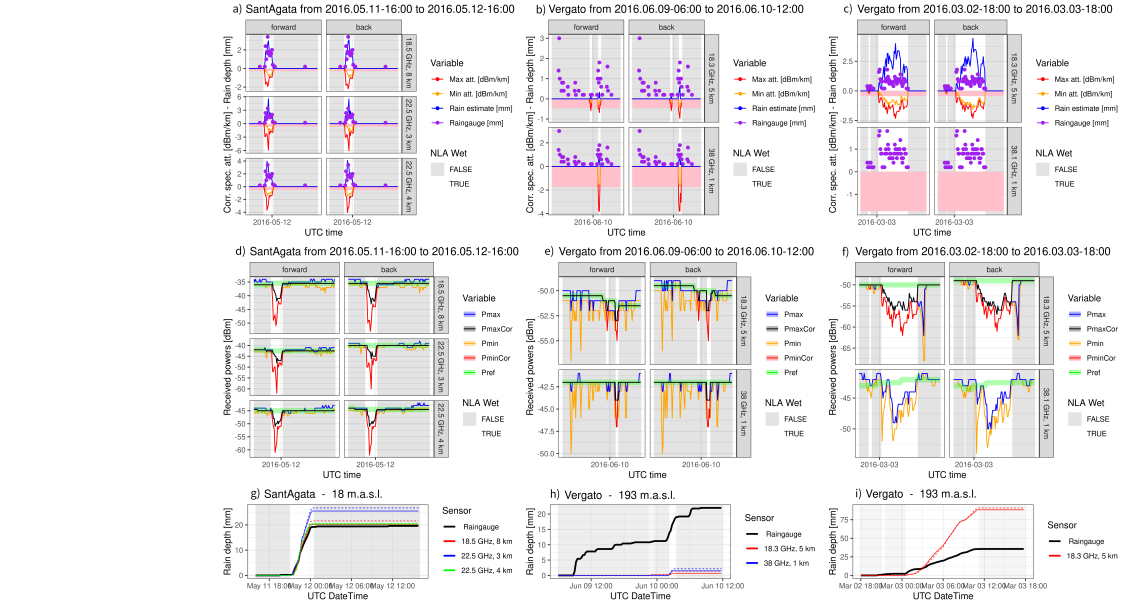

Figure 3. Case studies of the single link analysis; a), b) and c) show the specific attenuations (red, orange) and the rain estimates (purple) compared with the gauge measurements (blue dots), d), e) and f) the received signals, g), h) and (i) the cumulated rainfall amounts. Grey background corresponds to intervals labelled as dry by the NLA classification. Y axes resolutions are specific for each CML as received powers differ between different pathlengths.

https://doi.org/10.5194/amt-2020-43
Preprint. Discussion started: 27 February 2020

Atmospheric Measurement Techniques Discussions

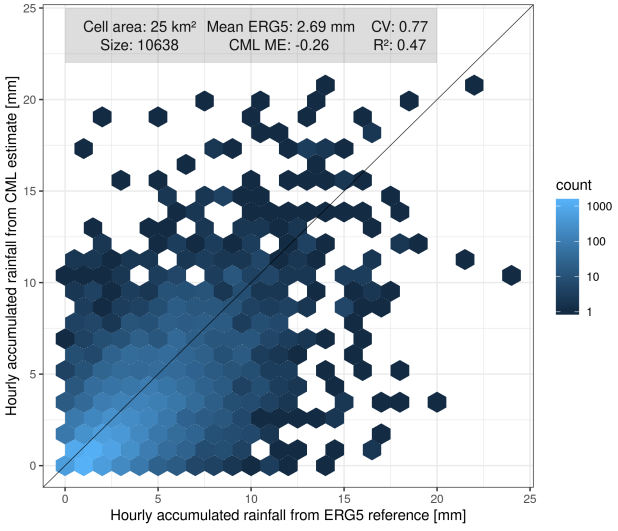

Figure 4. Hourly validation of link rainfall maps against ERG5 rainfall maps at grid box scale (highest resolution). Only the rainfall depths in which both CMLs and ERG5 measured > 0.1 mm were used. The black line is the y=x line.

https://doi.org/10.5194/amt-2020-43
Preprint. Discussion started: 27 February 2020

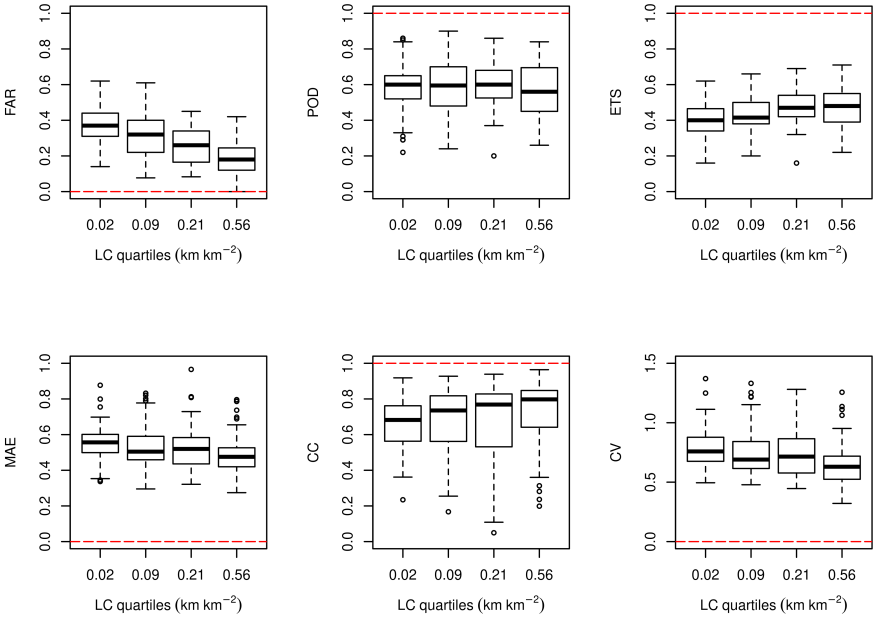

Figure 5. Distributions of four statistical indicators computed for every grid box and grouped in boxplots by quartiles of the link coverage LC (labelled by the quartiles centre). Red dashed lines are the optimal values for each score.

https://doi.org/10.5194/amt-2020-43
Preprint. Discussion started: 27 February 2020

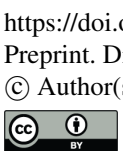

Atmospheric Measurement Techniques Discussions

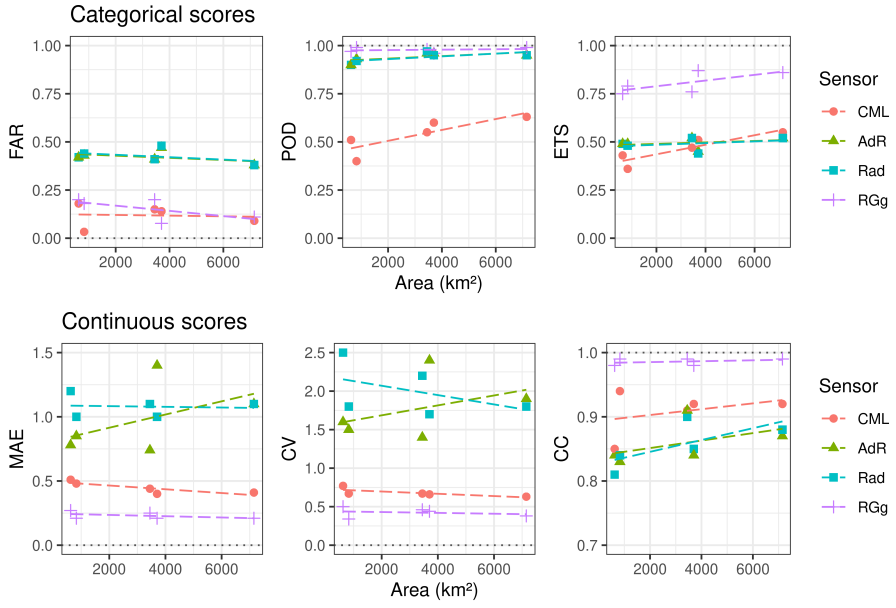

Figure 6. Scores of the areal-averaged rainfall amounts grouped per sensor and plotted against basin area. Linear fits are highlighted with dashed lines. The CML scores are indicated also numerically in Table 4.

https://doi.org/10.5194/amt-2020-43
Preprint. Discussion started: 27 February 2020

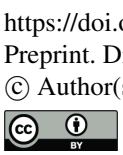

Atmospheric Measurement Techniques Discussions

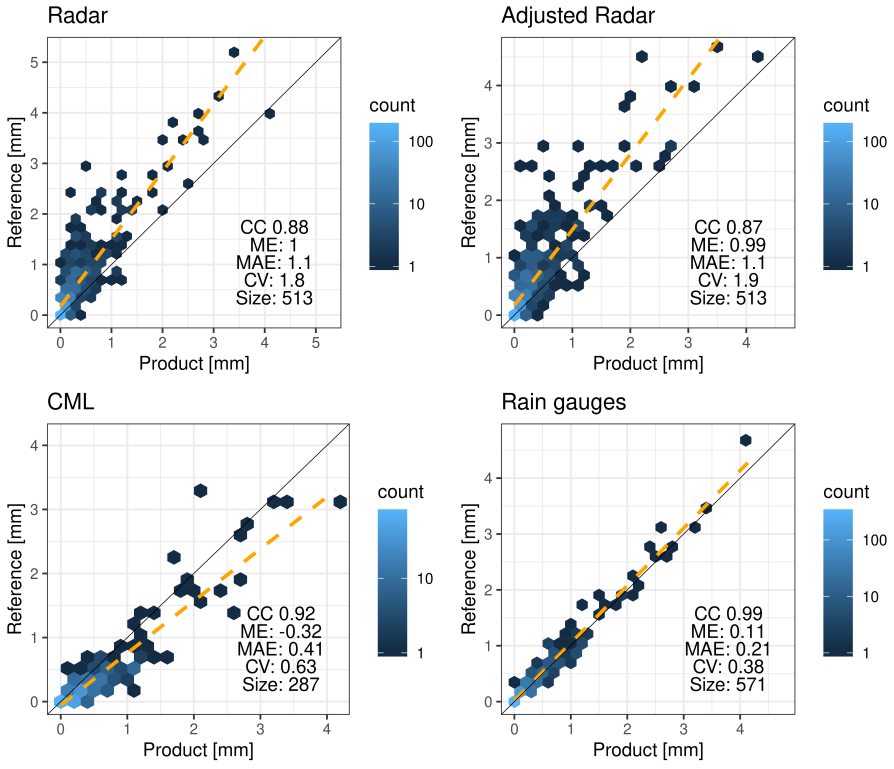

Figure 7. Comparison of hourly areal-averaged rainfall depths from the four products against the ERG5 reference. The total area (TA) wet-wet hours are considered.

https://doi.org/10.5194/amt-2020-43
Preprint. Discussion started: 27 February 2020

Atmospheric Measurement Techniques Discussions

Table 1. CML datasets comparison.

Variable	Unit	ER	NL	Overeem et al. (2013)	Overeem et al. (2016b)
Total area	km^2	7149	35500	35500	35500
CMLs	counts	319	1527	1514	2044
sub-links	counts	625	2473	2902	3383
LD	km^2	0.045	0.043	0.043	0.058
LL	km	6.0	2.9	3.1	3.6
BC	$\mathrm{km\,km}^{-2}$	0.27	0.13	0.13	0.21
$\overline{f}$	GHz	22.1	37.11	37-40	37-40

https://doi.org/10.5194/amt-2020-43
Preprint. Discussion started: 27 February 2020

Atmospheric Measurement Techniques Discussions

Table 2. Comparison with previous studies.

Variable	Unit	ER (present work)	Overeem et al. (2013)	Overeem et al. (2016b)
Total time window	-	2 months	3 months	2.5 years
Filter	-	Ref. AND Product > 0.1 $\mathrm{mm\ h^{-1}}$	Ref. OR Product > 0.1 $\mathrm{mm\ h^{-1}}$	Ref. > 0.1 $\mathrm{mm\ h^{-1}}$
Time scale	min	60	15	60
Gridbox area	$\mathrm{km^2}$	25	81	74
Reference	-	interpolated rain gauges	Gauge-adjusted radar	Gauge-adjusted radar
ME	-	-0.26	0.02	-0.16
CV	-	0.77	1.13	0.64
R^2	-	0.47	0.49	0.49

https://doi.org/10.5194/amt-2020-43
Preprint. Discussion started: 27 February 2020

Atmospheric Measurement Techniques Discussions

Table 3. Statistical indicators for each considered area, considering the highest resolution information (grid box scale), shown in ascending order of $\overline{LC}$. Continuous indicators are normalized and fractional. Values in bold (italics) are the best (worst) values in the column.

Area	$\overline{LC}$ (km km^{-2})	S (km^2)	FAR	POD	ETS	MB	ME	MAE	CV	CC
PP	0.17	3447	0.28	0.51	0.40	0.71	*-0.34*	*0.55*	*0.80*	*0.62*
TA	0.18	7149	0.30	0.54	0.42	0.77	-0.26	0.52	0.77	0.68
PRB	0.19	624	0.30	0.48	0.38	0.69	-0.31	0.50	0.76	0.67
BP	0.19	3702	*0.32*	**0.57**	**0.43**	**0.83**	**-0.19**	0.49	0.73	0.74
RRB	0.29	828	**0.16**	*0.39*	*0.35*	*0.47*	-0.31	**0.45**	**0.63**	**0.80**

https://doi.org/10.5194/amt-2020-43
Preprint. Discussion started: 27 February 2020

Atmospheric Measurement Techniques Discussions

Table 4. Values of the statistical indicators for the mean rain amounts over each considered area, shown in ascending order of surface area S. Values in bold (italics) are the best (worst) values in the column.

Area	S (km^2)	$\overline{LC}$ ($\mathrm{km\ km}^{-2}$)	FAR	POD	ETS	MB	ME	MAE	CV	CC
PRB	624	0.19	*0.18*	0.51	0.43	0.63	-0.36	*0.51*	*0.77*	*0.85*
RRB	828	0.29	**0.03**	*0.40*	*0.36*	*0.41*	*-0.43*	0.48	0.67	**0.94**
PP	3447	0.17	0.15	0.55	0.47	0.63	-0.37	0.44	0.67	0.91
BP	3702	0.19	0.14	0.60	0.51	**0.70**	**-0.23**	**0.40**	0.66	0.92
TA	7149	0.18	0.09	**0.63**	**0.55**	**0.70**	-0.32	0.41	**0.63**	0.92

https://doi.org/10.5194/amt-2020-43
Preprint. Discussion started: 27 February 2020

Atmospheric Measurement Techniques Discussions

Table 5. Latency and spatial and temporal sampling of the considered precipitation products.

Product	Reference time step (min)	Latency (min)	Spatial resolution (km)
CML	15	20	5
Radar raw	5	15	1
Radar adj.	60	60	1
Raingauges raw	60	60	-
ERG5	60	1440	5